ADVANCED ELECTRONIC MATERIALS
www.advelectronicmat.de

Pine-Branch-Like SnO_2/ZnO Heterostructure with Suppressed Dark Current and Enhanced On/Off Ratio for Visible-Blind UV Imaging

*Fa Cao, Li Su, Tingting Yan, Ziqing Li, Dmitry V. Shtansky, and Xiaosheng Fang**

In general, wide bandgap semiconductors (Eg > 3.0 eV) are sensitive to visible-blind ultraviolet (UV) radiation. However, a large dark current makes it difficult to implement efficient visible-blind sensing, which impedes their application in visible-blind UV image. In this work, pine-branch-like photodetectors (PDs) based on SnO_2/ZnO heterostructure are successfully fabricated. Compared with the high dark current (1.5×10^{-8} A) and low on/off ratio (42) of SnO_2 PD, the designed SnO_2/ZnO/4 (S/Z/4) PD shows a significantly reduced dark current (1.3×10^{-12} A), ultrahigh on/off ratio (16 405) under 300 nm UV illumination at 1 V bias. In addition, the UV/visible rejection ratio (R_{310}/R_{400}) of S/Z/4 PD is 1193, which is almost 48-times of that of SnO_2 PD (25). This shows great promise for application in visible-blind image sensors. The enhancement in performance is attributed to the formation of the type-II energy band structure, the low conductivity of ZnO layer, and the light trapping effect of pine-branch-like structure. Moreover, the SnO_2/ZnO/4 PD also exhibits fast response speed with a rising time of 0.48 ms and decay time of 2.07 ms, which exceeds most of the metal oxide-based PDs. The fabrication approach of pine-branch-like heterojunction can be extended to other one-dimensional materials for high-performance optoelectronic devices.

1. Introduction

The development of nanomaterials promotes the progress of modern optoelectronic industry. Among various widely studied nanomaterials (0D, 1D, and 2D materials), 1D nanomaterials with a large surface to volume ratio are receiving increased attention.[1] Ultraviolet photodetectors (UV PDs) based on 1D nanomaterials are of particular interest due to their enhanced responsivity and high photoconductive gain, and therefore, are widely used in space communication, image sensor, flame detection, etc.[1,2] However, commercially available Si-based UV PDs require expensive filters for its application in UV region. Thus, selecting suitable UV-only sensitive materials with special structure is a key factor for constructing a high performance visible-blind UV PDs.

Recently, visible-blind UV PDs based on wide bandgap semiconductors (ZnO, TiO_2, SnO_2, Ga_2O_3, etc.) have attracted great attention due to the importance of their application in ultraviolet astronomy and biological detection.[3–5] UV PDs based on these materials exhibit superior electric and optical properties. For example, a record high photo-to-dark current ratio of 3.3×10^5 and detectivity of 3.2×10^{12} Jones at an ultralow operation bias of 2 mV.[6] High responsivity of nearly 3 A W^{-1} was achieved in SnO_2-based microwires fabricated by electrospinning method.[2] However, UV PDs based on single metal oxide semiconductor suffer from high dark current and long response time, which may be caused by the oxygen related defects.[7–9] The large dark current reduces the sensitivity and UV/visible rejection ratio of the device. Many efforts have been undertaken to combine two materials into one specific geometric nanostructure to solve the large dark current and low UV/visible rejection ratio problems. For instance, novel Ω-shaped core-shell heterostructure based on SnO_2/ZnO exhibits reduced dark current and enhanced UV light current with a responsivity of 100 A W^{-1}.[2] Due to reduced dark current, the UV/visible rejection ratio of micrometric ZnO/AlN core–shell UV photodetectors has been increased from 453 to 11 000.[10] Although traditional core-shell heterostructure is beneficial for reducing dark current and promoting carriers separation, however, it cannot make full use of the incident light. Therefore, a novel core–shell structure with a light trapping effect is needed to fabricate UV PDs with low dark current, high on/off ratio, and enhanced UV/visible rejection ratio.

In order to meet the above requirements, through composition selection and structural design, a novel pine-branch-like SnO_2/ZnO heterostructure has been successfully fabricated. The SnO_2/ZnO-4 h (S/Z/4) PD exhibits significantly reduced dark current, enhanced on/off ratio and UV/visible rejection ratio (R_{310}/R_{400}) with a value of 1.3×10^{-12} A, 16 405 and 1193, respectively. In addition, the S/Z/4 PD with a fast rise time of 0.48 ms and a decay time of 2.07 ms can be well applied in the visible-blind UV imaging areas. The design of such a light-harvesting structure can be expanded to other optoelectronic devices.

F. Cao, L. Su, T. T. Yan, Z. Q. Li, X. S. Fang
Department of Materials Science
Fudan University
Shanghai 200433, P. R. China
E-mail: xshfang@fudan.edu.cn
D. V. Shtansky
National University of Science and Technology "MISIS"
Moscow 119049, Russian Federation

The ORCID identification number(s) for the author(s) of this article can be found under https://doi.org/10.1002/aelm.202101373.

DOI: 10.1002/aelm.202101373

2. Results and Discussion

The structure and phase composition of SnO_2 and SnO_2/ZnO samples were characterized by XRD and the corresponding XRD patterns are shown in Figure S1 (Supporting Information). For SnO_2 microwires, twelve peaks observed at 26.58°, 33.56°, 37.94°, 38.96°, 51.76°, 54.74°, 57.8°, 62.58°, 64.71°, 65.94°, 71.25°, and 78.68° are well matched with the (110), (101), (200), (111), (211), (240), (002), (221), (112), (301), (202), and (321) planes of tetragonal SnO_2 (JCPDS # 99-0024), respectively.[11] For SnO_2/ZnO composites, additional peaks observed at 31.76°, 34.42°, 36.25°, 56.6°, 68.13° are assigned to the (100), (002), (101), (110), and (112) planes of hexagonal ZnO (JCPDS # 36-1451), respectively.[12] The intensity of ZnO XRD peaks increased with increasing growth time, which may be due to an increase in the amount of ZnO. No diffraction peaks from other phases were detected, indicating the high purity of SnO_2 and ZnO materials.

The morphology of SnO_2 microwires and SnO_2/ZnO composites was analyzed by SEM, and the obtained results are shown in **Figure 1**b–e. The SEM (Figure 1b) and TEM images (Figure S2, Supporting Information) show single crystal SnO_2 microwires with an average diameter of 150–300 nm and smooth surface. ZnO nanobranches were grown on SnO_2 microwires by hydrothermal method. Figure 1c–e exhibits the SEM images of SnO_2/ZnO composites with growth time of 2, 4, and 6 h, respectively. At a growth time of 2 h, branched ZnO nanorods grown on SnO_2 nanowires can be observed (Figure 1c). When the growth time increases to 4 h, pine-branch-like SnO_2/ZnO composites are clearly seen. The average diameter and length of ZnO branches are about 150 nm and 1.4 µm, respectively (Figure 1d). With longer growth time of 6 h, the average diameter and length of ZnO branches increased to 200 nm and 2 µm (Figure 1e). Figure 1f–i shows Sn, Zn, and O elemental mapping. Sn distributes uniformly over the main stem of nanostructure, while the distribution of Zn and O follows the shape of ZnO branches. Thus, the pine-branch-like SnO_2/ZnO composites composed of SnO_2 stem and ZnO branches.

The photo-response performance of SnO_2 and SnO_2/ZnO PDs were tested individually. **Figure 2**a is a scheme of the PDs, and Figure 2b shows characteristic *I–V* curves of SnO_2 and S/Z/4 PDs (*I–V* curves of all PDs are shown in Figure S3, Supporting Information). When the SnO_2 microwires were covered with ZnO nanobranches, the dark current reduced from 10^{-8} A (S PD) to 10^{-12} A (S/Z/4 PDs). The circuit diagrams of SnO_2 and SnO_2/ZnO PDs are presented in Figure S4 (Supporting Information). In the presence of ZnO nanobranches, the resistance of the circuit is enhanced, which contributes to the reduced dark current. The significantly reduced dark current is mainly due to the low conductivity of ZnO, as proven by the ZnO *I–V* curves (Figure S5, Supporting Information). Time-dependent response of PDs was measured under 300 nm light (1.14 mW cm^{-2}, 1 V) via switching on and off the light source periodically. The *I–T* curves of all the PDs under 1 V bias show excellent stability and periodicity (Figure 2c). Owing to the reduced dark current, the on/off ratio is significantly enhanced from 42 (SnO_2 PD) to 16 405 (S/Z/4 PD) (Figure S6, Supporting Information). It is worth noting that when the growth time of ZnO branches

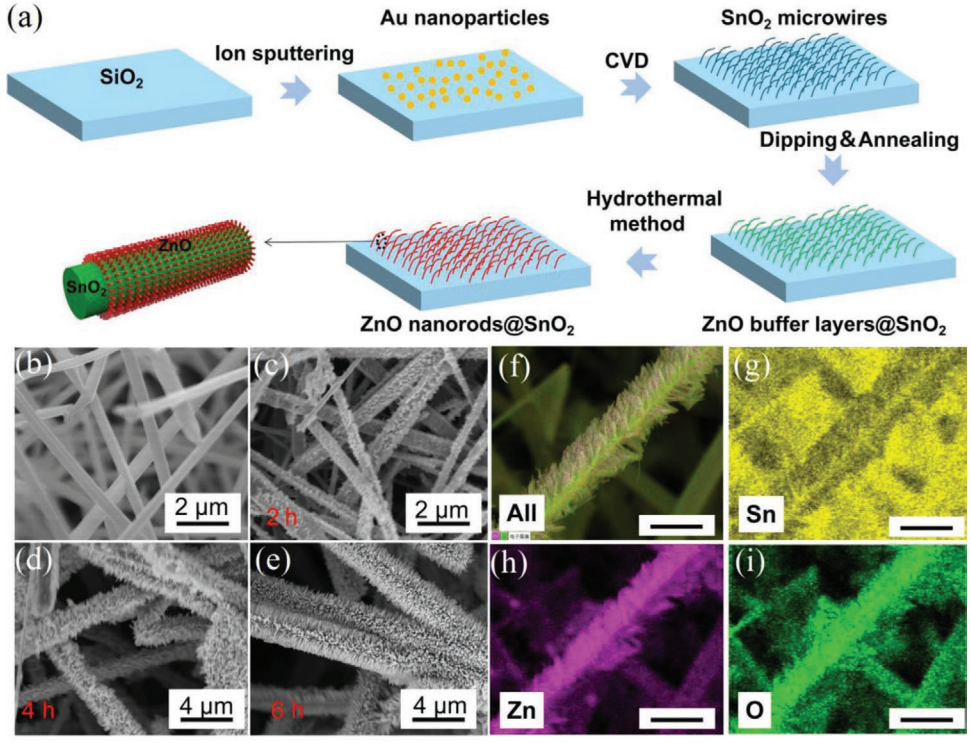

Figure 1. a) Schematic of fabrication process of pine-branch-like SnO_2/ZnO heterostructure. b) SEM image of SnO_2 microwires. SEM images of SnO_2/ZnO heterojunctions, c) SnO_2/ZnO-2 h, d) SnO_2/ZnO-4 h, e) SnO_2/ZnO-6 h. f–i) EDS elemental maps corresponding to (d) (scale bar 4 µm).

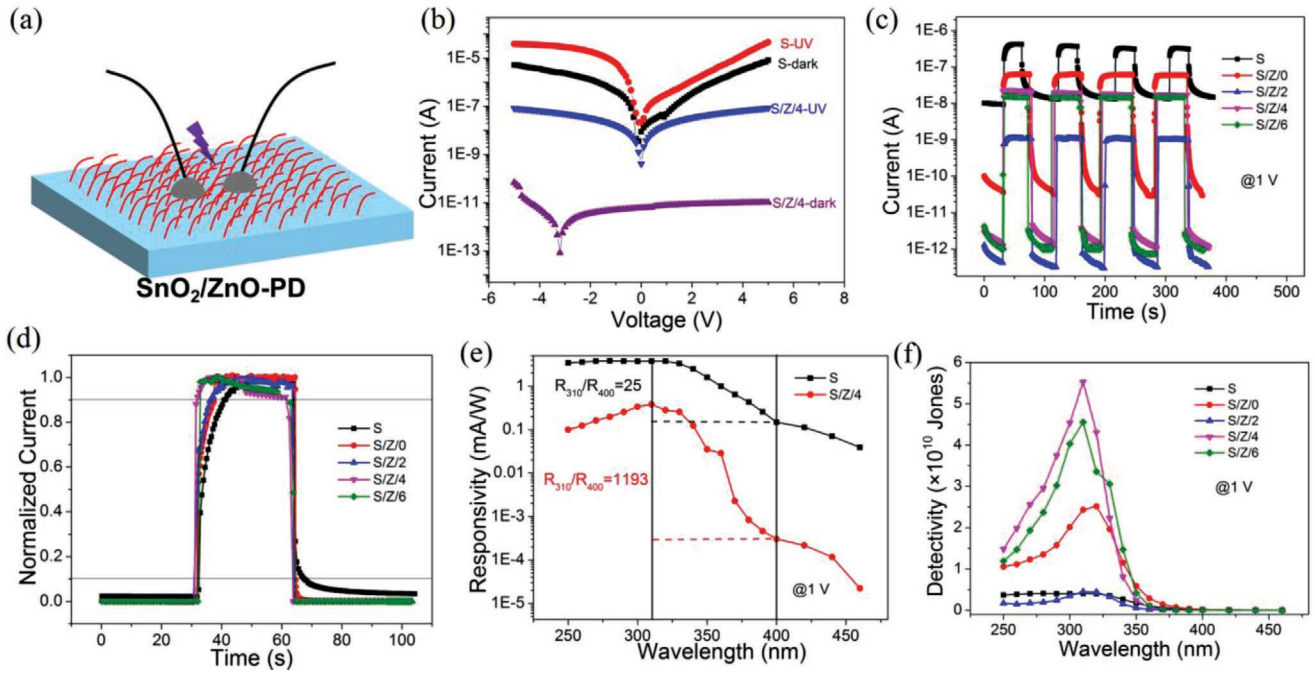

Figure 2. a) Schematic of SnO_2/ZnO based PDs. b) *I–V* curves of SnO_2 and S/Z/4 PDs in the dark and under 300 nm light irradiation (1.44 mW cm^{-2}). c) Transient response of the PDs at 300 nm light irradiation (1.44 mW cm^{-2}) at 1 V bias. d) The normalized IT curves of the PDs. e,f) Spectra response of the PDs at 1 V bias.

is increased from 2 to 4 h and further to 6 h, the photocurrent increases from 10^{-9} to 10^{-8} A. This may be because well-aligned ZnO nanoarrays have light trapping effect making full use of the incident light. Representative responsivity (R) and detectivity (D^*) parameters are employed to examine the photodetecting performance of PDs. R denotes the efficiency of PD in response to optical signals, and D^* indicates the ability to detect weak signals. They can be calculated from following formula (1) and (2) as follows:[13,14]

$$R = \frac{I_l - I_d}{AP} \tag{1}$$

$$D^* = \frac{RA^{1/2}}{(2eI_d)^{1/2}} \tag{2}$$

where I_l and I_d are the light and dark currents; A is the effective area under illumination (0.04 cm^2), P represents the incident light power density, and e is the electron charge (1.6×10^{-19} C). The S/Z/4 PD displays much better sensitivity, on/off ratio and UV/visible rejection ratio (R_{310}/R_{400}) than most reported PDs as illustrated in **Table 1**.

Fast response speed to light signal is essential to a high PD performance. To investigate the influence of branched ZnO nanorods on the response speed of SnO_2/ZnO PDs, the *I–T* curves of PDs are normalized and depicted in Figure 2d. The measured rise and decay times of SnO_2 PD are about 9.01 and 3.46 s, respectively. When decorating with ZnO branches, the rise and decay times of the representative S/Z/4 PD were reduced to 0.42 and 1.14 s, respectively. It demonstrates that the junctions between SnO_2 and ZnO can facilitate the separation of photo-generated electrons.

The UV/visible rejection ratio is an essential parameter to assess the ability of a PD to exclude the visible light interference, which can efficiently expand the application of UV PDs. The spectral responsivity was determined to evaluate the UV/visible rejection ratio (R_{310}/R_{400}) of S and S/Z/4 PD, as shown in Figure 2e. In the presence of ZnO branches, the UV/visible

Table 1. Comparison of the main parameters of as-fabricated PDs with literature data.

Device	λ [nm]	Bias [V]	On/off	Responsivity [mA W^{-1}]	R_{UV}/R_{vis}	Rise/fall time	Ref.
ZnO nanofiber	350	5	<10	–	<100	19.5/45.2 s	[15]
Micro-ZnO/Mxene	365	5	<1	5050	–	1.6/4 s	[16]
ZnO/AlN	193	5	300	381 000	–	0.12/0.36 s	[10]
ZnO/CuI/Au	365	1	<1	–	<100	≈4/14 s	[17]
ZnO/BiOCl/TiC	350	5	7996	0.094	–	2.59/0.93 s	[18]
Ω-shaped SnO_2/ZnO	250	5	10^4	100 000	≈10^3	120/110 s	[2]
Pine-branch-like SnO_2/ZnO	300	1	16 405	0.35	1193	0.48/2.07 ms	This work

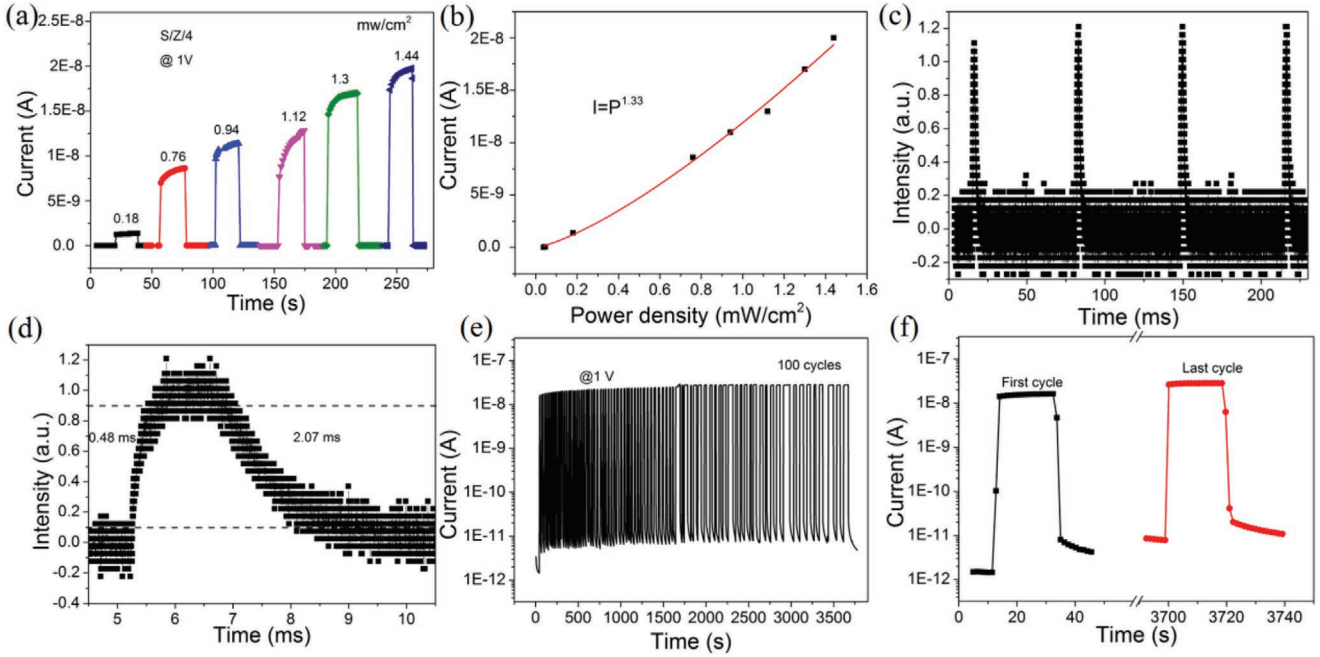

Figure 3. a) *I–T* curves of S/Z/4 PD under 300 nm light irradiation at different light intensities. b) Photocurrent of S/Z/4 PD as a function of light intensity. c,d) Pulse response of S/Z/4 PD. e) *I–T* curve of S/Z/4 PD with 100 cycles at 1 V bias. f) First and last cycles of *I–T* curves of S/Z/4 PD.

rejection ratio (R_{310}/R_{400}) increases from 25 (SnO_2) to 1193 (S/Z/4), demonstrating that the S/Z/4 PD has huge application prospects in the visible-blind UV PDs. Figure 2f shows the spectral D^* values of *S* and S/Z PDs. When decorating with ZnO branches, the D^* of PD increased from 3.7×10^9 (SnO_2 PD) to 5.4×10^{10} (S/Z/4 PD) Jones, which is attributed to the reduced dark current.

Figure 3a,b are the time-dependent response of the S/Z/4 PD under different light power densities, respectively. It can be seen that the PD photocurrent of S/Z/4 sample increases with increasing light power density. The on/off ratio reaches the maximum value of 16 405 when the light intensity is 1.44 mW cm^{-2}. The dependence of photocurrent on light intensity can be fitted by Equation (3):[19]

$$I_1 \sim P^{\theta} \tag{3}$$

where I_1 refers to photocurrent. Generally, θ is between 0 and 1 for various PDs. However, the fitted θ of S/Z/4 PD is 1.33, as shown in Figure 3b, which can be explained by the pine-branch-like SnO_2/ZnO structure that can trap more incident light. The pulse response of S/Z/4 PD was further characterized to better understand the time-resolved property. The measurement system is shown in Figure S7 (Supporting Information). Figure 3c,d are the pulse response of S/Z/4 PD. The S/Z/4 PD illustrates a stable transient response capability with short rising and decay times of 0.48 and 2.07 ms, respectively, which outperforms most metal oxide semiconductor-based PDs. To evaluate the cyclic stability of S/Z/4 PD, continuous *I–T* test was performed by turning on and off the UV light periodically, as shown in Figure 3e. The obtained results indicate the perfect device stability. The *I–T* curves of the first and the last cycles are displayed in Figure 3f. The PD shows unreduced photocurrent after 100 continuous test cycles, demonstrating its excellent UV resistance. The photocurrent is a little enhanced, which may own to the desorption of the O^{2-}. When the PD is illuminated by UV light, photogenerated electrons will be captured by O^{2-} which will reduce the resistance of the PD, so the photocurrent is increased. Based on the above results, the S/Z/4 PD fabricated in this work shows great promise for applications in optical instruments for detecting and imaging visible-blind UV radiation.

An imaging system was constructed to investigate the visible-blind imaging capability of our PDs, as illustrated in **Figure 4**a.[20] A hollow template with F graphics (2.5 × 3 cm) was placed between the light and the PDs, which was used to collect the light signal. The template can be moved continuously in horizontal and vertical direction (X and Y direction), as shown in Figure 4b. The photocurrent from the PDs was collected by a Keithley 4200 and then was analyzed by a computer. A 5 × 7 pixels' 300/400 nm image was obtained, via transforming the output signal current (Figures S8 and S9, Supporting Information) into "gray code" (Figure 4c,d). The imaging results of SnO_2 PD are shown in Figure 4c. The image "F" was displayed in both 300 and 400 nm illumination with a gray value ratio (the photocurrent of PD under 300 nm light vs the photocurrent of PD under 400 nm light) 20:1. When decorated with ZnO branches, the image result "F" of S/Z/4 PD can only be seen under 300 nm UV illumination (Figure 4d), demonstrating its high visible-blind photodetecting performance. The results show that in the presence of ZnO branches, the defect-related visible response is suppressed, leading to the enhanced UV/visible rejection ratio.

PL, UV–vis and XPS valence band spectra were obtained and analyzed to understand the mechanism of photodetecting performance of the S/Z PDs. Figure 5a demonstrates the PL

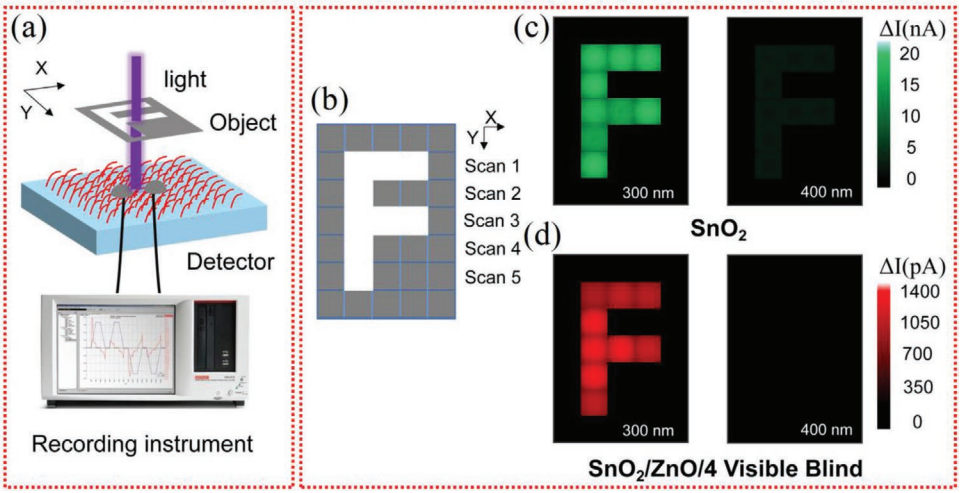

Figure 4. a) Schematic diagram for the imaging system employing the photodetector as imaging pixel. b) The moving direction of the object. c,d) The images of SnO_2 and SnO_2/ZnO/4 PD under 300 and 400 nm light irradiation, respectively.

spectra of SnO_2 and SnO_2/ZnO samples. The pristine SnO_2 microwires exhibit visible emission peaked at about 600 nm, which is related to surface oxygen defects.[21] However, when the surface of SnO_2 microwires was modified by ZnO, the emission peaks centered at 600 nm is reduced. This may be due to a decrease in the number of oxygen defects and an enhanced separation efficiency of the photo-generated carriers. Thus, the photo-generated carriers can be fully utilized.

The UV–vis spectra of SnO_2, ZnO and SnO_2/ZnO samples recorded in the range of 250–800 nm are illustrated in **Figure 5**b. The SnO_2 and ZnO exhibit sharp absorption edge at about 310 and 370 nm, respectively, indicating that they may respond to UV light for photodetecting application.[22–24] Two absorption edges at 310 and 370 nm can be observed from SnO_2/ZnO, which are well-matched with that of ZnO and SnO_2 constituents, respectively. Moreover, the UV absorption of SnO_2/ZnO is increased and visible absorption is reduced which contributes to the enhanced UV/visible rejection ratio. The superior UV absorption may be attributed to the light trapping effect of the nanorod array of ZnO nano-branches, as shown in

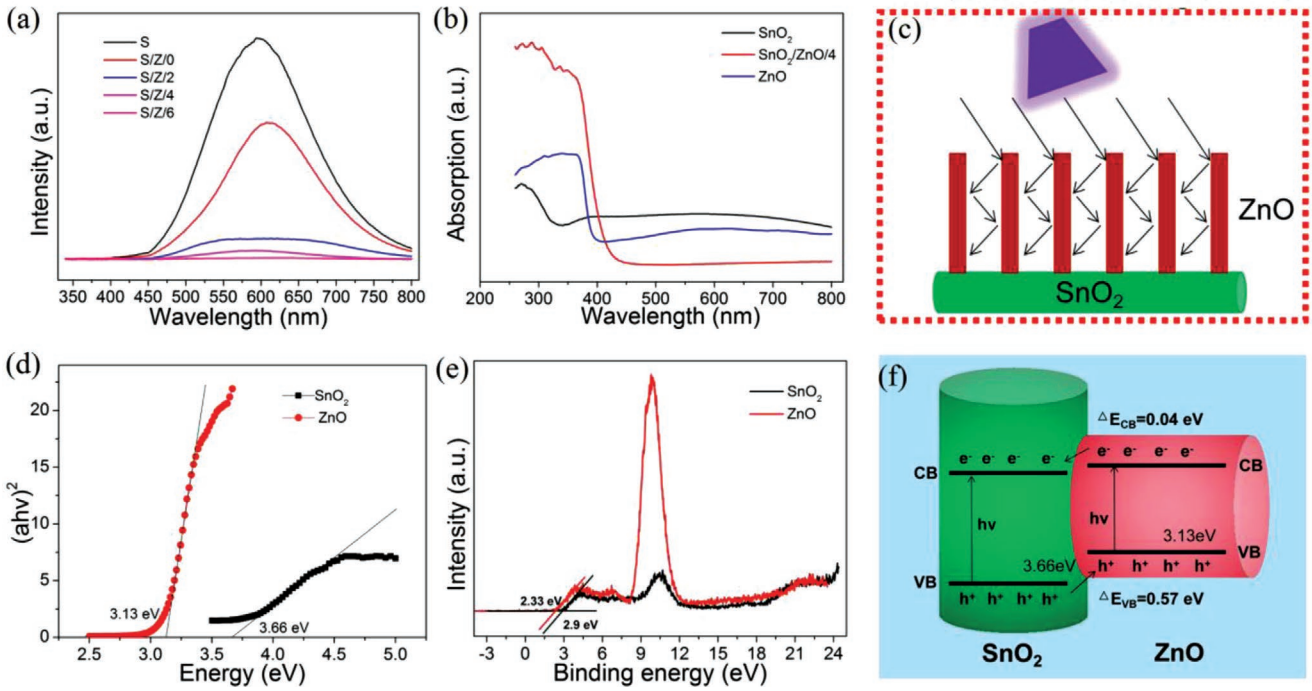

Figure 5. a) PL spectra of SnO_2 and SnO_2/ZnO samples. b) UV–vis absorption spectra of SnO_2 and SnO_2/ZnO-4 h and ZnO samples. c) Schematic of the light trap effect of SnO_2/ZnO PD. d) The plot of $(\alpha h\nu)^2$ versus photon energy of SnO_2 and ZnO. e) XPS valence band spectra of SnO_2 and ZnO. f) Energy band diagram of SnO_2 and ZnO and the moving direction of the carriers under UV light.

Figure 5c. To confirm the conduction band offset (ΔE_{CB}) of the SnO_2 and ZnO, the optical bandgaps of SnO_2 and ZnO microwires were determined by Equation (4):[25]

$$(\alpha h\nu)^2 = A\left(h\nu - E_{gap}\right) \quad (4)$$

α is the absorption coefficient, $h\nu$ is the photon energy, A is the constant. The straight line between $(\alpha h\nu)^2$ and $h\nu$ attained in Figure 5d demonstrates that the bandgaps of SnO_2 and ZnO are 3.66 and 3.13 eV, respectively.

The high-resolution XPS valence band spectra of SnO_2 and ZnO started at 2.9 and 2.33 eV, respectively, as shown in Figure 5e, and the valence band offset (ΔE_{VB}) of SnO_2 and ZnO is 0.57 eV. Thus, the conduction band offset (ΔE_{CB}) of SnO_2 and ZnO is 0.04 eV. The band energy alignment of the SnO_2 and ZnO junction is illustrated in Figure 5f. Type-II heterojunction has formed between SnO_2 and ZnO, and the electrons and holes can be generated and move in opposite directions when illuminated with UV light.

3. Conclusion

In summary, pine-branch-like photodetectors (PDs) based on SnO_2/ZnO heterostructure are successfully prepared. The S/Z/4 PD demonstrates significantly reduced dark current from 1.5×10^{-8} A to 1.3×10^{-12} A. The on/off ratio and UV/visible rejection ratio (R_{310}/R_{400}) of S/Z/4 PD are 16405 and 1193, which are 391 and 47.7 times higher than those of SnO_2 PD (42 and 25, respectively). In addition, the S/Z/4 PD exhibits a fast response speed with a rise time of 0.48 ms and a decay time of 2.07 ms, which is faster than most reported SnO_2 and ZnO-based UV PDs. The S/Z/4 PD also shows great promise in visible-blind UV imaging areas. The design of such light-harvesting structure can be further expanded to other optoelectronic devices.

4. Experimental Section

Materials Fabrication: SnO_2 microwires were prepared on SiO_2 substrate by chemical vapor deposition (CVD) method. Briefly, Au nanoparticles with a size of 5–10 nm were sputtered on SiO_2 as a buffer layer. The substrate was put on the quartz boat with 0.5 g Sn particles (99.9%). The reaction chamber was firstly cleaned by pure N_2 to remove residual oxygen and then heated to 800 °C at a constant N_2 flow rate of 100 sccm (standard cubic centimeters per minute). Subsequently, 5 sccm of O_2 were added to the chamber immediately and the temperature was increased to 950 °C. After that, the system was cooled down to room temperature naturally.

ZnO nanorods (NRs) were fabricated by hydrothermal method. In short, the above fabricated SnO_2 microwires were immersed in a ZnO sol–gel solution for 2 min and annealed at 200 °C for 1 h to obtain a ZnO buffer layer. ZnO NRs were prepared by a hydrothermal process in an aqueous solution containing 0.2 M zinc nitrate hexahydrate [$Zn(NO_3)_2{\cdot}6H_2O$] and hexamethylenetetramine (HMTA) at 90 °C for 0, 2, 4, and 6 h. The corresponding PDs are denoted as S, S/Z/2, S/Z/4, and S/Z/6. The schematic of fabrication process of the pine-branch-like SnO_2/ZnO heterostructure is illustrated in Figure 1a.

Materials Characterization and Photoelectric Measurement: Field-emission electron microscopy (FEI Nova NanoSEM 430) and transmission electron microscopy (TEM, JEOL2100F) were used for morphology analysis. An X-ray diffractometer (XRD, Cu-Kα radiation source, λ = 0.15418 nm) was used for crystal phase determination. Optical information was collected by an UV–vis spectrophotometer (UV2450, Shimadzu) and a FLS920 fluorescence spectrometer with a 325 nm He-Cd laser as an excitation source.

Two pieces of silver pastes (0.2 × 0.2 cm) with a distance of 0.2 cm were brushed on the samples as two PD electrodes. The current–voltage (I–V) characteristic and the current–time (I–T) transient response were obtained using a program-controlled semiconductor characterization system (Keithley 4200S, USA). The light source was a 450 W Xe lamp equipped with a monochromator, and the light intensity was measured by a NOVA II power meter (OPHIR photonics). The PD pulse response time was evaluated by an Nd:YAG 355 nm pulsed laser (repetition rate 15 Hz, pulse width: 5 ns) and a digital oscilloscope (Tektronix DPO 5140B).

Supporting Information

Supporting Information is available from the Wiley Online Library or from the author.

Acknowledgements

The authors would like to thank Dr. Jiaxin Chen for her kind suggestions. This work was supported by National Natural Science Foundation of China (Nos. 12061131009 and 51872050), the young scientist project of MOE innovation platform, Science and Technology Commission of Shanghai Municipality (Nos. 21520712600 and 19520744300), and the China Postdoctoral Science Foundation (KLH2021078). D.V.S. gratefully acknowledges the financial support from the Russian Science Foundation (No. 21-49-00039).

Conflict of Interest

The authors declare no conflict of interest.

Data Availability Statement

The data that support the findings of this study are available from the corresponding author upon reasonable request.

Keywords

pine-branch-like, reduced dark current, SnO_2/ZnO heterostructure, visible-blind

Received: December 20, 2021
Revised: February 1, 2022
Published online:

[1] a) W. X. Ouyang, J. X. Chen, Z. F. Shi, X. S. Fang, *Appl. Phys. Rev.* **2021**, *8*, 031315; b) M. Y. Liao, *Funct. Diamond* **2021**, *1*, 29.
[2] M. X. Hu, F. Teng, H. Y. Chen, M. M. Jiang, Y. Z. Gu, H. L. Lu, L. F. Hu, X. S. Fang, *Adv. Funct. Mater.* **2017**, *27*, 1704477.
[3] a) Y. F. Wang, L. Li, H. B. Wang, L. X. Su, H. Y. Chen, W. P. Bian, J. G. Ma, B. S. Li, Z. G. Liu, A. D. Shen, *Nanoscale* **2019**, *12*, 1406; b) Z. L. Li, Z. Q. Li, C. L. Zuo, X. S. Fang, *Adv. Mater.* **2022**, *34*, 2109083.

[4] D. D. Hao, D. P. Liu, Y. K. Shen, Q. Q. Shi, J. Huang, *Adv. Funct. Mater.* **2021**, *31*, 2100773.
[5] a) M. X. Chen, B. Zhao, G. F. Hu, X. S. Fang, H. Wang, L. Wang, J. Luo, X. Han, X. D. Wang, C. F. Pan, Z. L. Wang, *Adv. Funct. Mater.* **2018**, *28*, 1706379; b) T. T. Yan, S. Cai, Z. J. Hu, Z. Q. Li, X. S. Fang, *J. Phys. Chem. Lett.* **2021**, *12*, 9912.
[6] a) R. H. Bo, N. Nasiri, H. J. Chen, D. Caputo, L. Fu, A. Tricoli, *ACS Appl. Mater. Interfaces* **2017**, *9*, 2606; b) N. Nasiri, R. Bo, L. Fub, A. Tricoli, *Nanoscale* **2017**, *9*, 2059.
[7] a) E. Pargoletti, U. H. Hossain, I. D. Bernardo, H. Chen, T. Tran-Phu, G. L. Chiarello, J. Lipton-Duffin, V. Pifferi, A. Tricoli, G. Cappelletti, *ACS Appl. Mater. Interfaces* **2020**, *12*, 39549; b) N. Nasiri, R. Bo, H. J. Chen, T. P. White, L. Fu, A. Tricoli, *Adv. Opt. Mater.* **2016**, *4*, 1787.
[8] S. Y. Li, Y. Zhang, W. Yang, H. Liu, X. S. Fang, *Adv. Mater.* **2020**, *32*, 1905443.
[9] F. Teng, W. X. Ouyang, Y. Li, L. X. Zheng, X. S. Fang, *Small* **2017**, *13*, 1700156.
[10] D. T. You, C. X. Xu, J. Zhao, F. F. Qin, W. Zhang, R. Wang, Z. L. Shi, Q. N. Cui, *Adv. Opt. Mater.* **2019**, *7*, 1801522.
[11] L. L. Zhu, M. H. Hong, G. W. Ho, *Sci. Rep.* **2015**, *5*, 11609.
[12] Ü. Özgür, Y. I. Alivov, C. Liu, A. Teke, M. A. Reshchikov, S. Doğan, V. Avrutin, S. J. Cho, H. Morkoç, *J. Appl. Phys.* **2005**, *98*, 041301.
[13] M. I. Saleem, S. Y. Yang, A. Batool, M. Sulaman, C. P. Veeramalai, Y. R. Jiang, Y. Tang, Y. Y. Cui, L. B. Tang, B. S. Zou, *J. Mater. Sci. Technol.* **2021**, *75*, 196.
[14] Y. Yuan, Z. Ji, G. H. Yan, Z. W. Li, J. L. Li, M. Kuang, B. Q. Jiang, L. L. Zeng, L. K. Pan, W. J. Mai, *J. Mater. Sci. Technol.* **2021**, *75*, 39.
[15] Z. M. Zhang, Y. Ning, X. S. Fang, *J. Mater. Chem. C* **2019**, *7*, 223.
[16] F. Cao, Z. H. Pan, X. H. Ji, *J. Appl. Phys.* **2021**,*129*, 204503.
[17] F. Cao, L. Jin, Y. Wu, X. H. Ji, *J. Alloys Compd.* **2021**, *859*, 158383.
[18] W. X. Ouyang, J. X. Chen, J. H. He, X. S. Fang, *Adv. Electron. Mater.* **2020**, *6*, 2000168.
[19] J. Y. Wang, L. F. Huang, K. X. Jin, W. Tian, *APL Mater.* **2018**, *6*, 076106.
[20] L. Li, H. Y. Chen, Z. M. Fang, X. Y. Meng, C. T. Zuo, M. L. Lv, Y. Z. Tian, Y. Fang, Z. Xiao, C. X. Shan, Z. Xiao, Z. W. Jin, G. Z. Shen, L. Shen, L. M. Ding, *Adv. Mater.* **2020**, *32*, 1907257.
[21] M. Aslam, M. T. Qamar, S. Ali, A. U. Rehman, M. T. Soomro, I. Ahmed, I. M. I. Ismail, A. Hameed, *J. Environ. Manage.* **2018**, *217*, 805.
[22] G. L. Lan, J. P. Nong, W. F. Jin, R. R. Zhu, P. Luo, H. B. Jiang, W. Wei, *Surf. Coat. Technol.* **2019**, *359*, 90.
[23] W. X. Ouyang, F. Teng, M. M. Jiang, X. S. Fang, *Small* **2017**, *13*, 1702177.
[24] Y. H. Chen, L. X. Su, M. M. Jiang, X. S. Fang, *J. Mater. Sci. Technol.* **2022**, *105*, 259.
[25] S. Wu, Z. W. Chen, T. Wang, X. H. Ji, *Appl. Surf. Sci.* **2017**, *412*, 69.